Nano Research 2015, 8(9): 2970–2977
DOI 10.1007/s12274-015-0802-2
Research Article
ISSN 1998-0124
CN 11-5974/O4

Strong tunability of cooperative energy transfer in Mn^{2+}-doped (Yb^{3+}, Er^{3+})/$NaYF_4$ nanocrystals by coupling with silver nanorod array

Yalan Wang[1], Fan Nan[1], Ziqiang Cheng[1], Junbo Han[2], Zhonghua Hao[1], Hongxing Xu[3] (✉), and Ququan Wang[1] (✉)

[1] *Department of Physics, Wuhan University, Wuhan 430072, China*
[2] *Wuhan National High Magnetic Field Center, Huazhong University of Science and Technology, Wuhan 430074, China*
[3] *The Center for Nanoscience and Nanotechnology, the School of Physics and Technology & the Institute of Advanced Research, Wuhan University, Wuhan 430072, China*

Received: 3 February 2015
Revised: 21 April 2015
Accepted: 23 April 2015

KEYWORDS
surface plasmon resonance, rare-earth nanocrystal, silver nanorod array, upconversion photoluminescence, cooperative energy transfer

ABSTRACT

Fluorescent rare-earth ions are useful for efficient energy transfer via multi-channels with different properties. Tuning these transfer processes in functional rare-earth materials has attracted considerable attention to satisfy the various demands of diverse practical applications. In this study, strong tunabilities of cooperative energy transfer and nonlinear upconversion emissions are realized using (Yb^{3+}, Er^{3+})/$NaYF_4$ nanocrystals with and without doped Mn^{2+} ions by adopting a plasmonic nanocavity composed of a silver nanorod array. The plasmon nanocavity can not only increase the energy transfer between Mn^{2+} and (Yb^{3+}, Er^{3+}) but also significantly enhance the radiative emission. This reveals a prominent nonlinear gain in the nanocavity nanosystems. These observations suggest the prospective applications in the design and preparation of rare-earth nanocrystals with excellent tunabilities of multiple functionalities.

1 Introduction

Fluorescent rare-earth ions have attracted significant attention due to their excellent optical properties such as highly efficient fluorescence ranging from violet to near infrared wavelengths, very large Stokes shift, and long fluorescence lifetime. They also have great potential applications in bioimaging and for the construction of compact solid lasers, solar cells, and lighting and color displays [1–12]. The near-infrared-to-visible multicolor upconversion emission of rare-earth ions has proven valuable in the fields of solar photovoltaic technology and multiplexed biological labeling [13–18]. The most important issue in such

Address correspondence to Ququan Wang, qqwang@whu.edu.cn; Hongxing Xu, hxxu@iphy.ac.cn

applications is to fine-tune the various energy transfer processes between rare-earth ions. These processes include cooperative energy transfer [19–23], energy migration [24, 25], and cross energy relaxation [26]. For instance, paramagnetic Mn^{2+} ions can be used to manipulate the cooperative energy transfer and adjust the fluorescence spectrum of (Yb^{3+}, Er^{3+}) co-doped composites. This results in a suppressed green emission and an enhanced red emission [19, 20].

Surface plasmon resonances of metallic nanostructures strongly enhance the interactions between light and matter (including light absorption, energy transfer, and radiative emissions) at the nanometer scale. This is widely used to tune the fluorescence intensity and emission spectrum of organic molecules, semiconductor quantum dots, and rare-earth nanocrystals [27–39]. Recently, significant resonant enhancement of rare-earth nanocrystal photoluminescence (PL) intensity (~35 fold) has been achieved by employing a Au nanohole array with precisely controlled periodicity that is resonant with the excitation wavelength of the upconversion [33–40].

Surface plasmon polariton (SPP) waves have been used to resonantly enhance the upconversion PL in doped lanthanide nanocrystals. This has been demonstrated using a specially designed Au pyramid array that enables further adjustment of the emission spectra due to the metal-mediated quenching of the green fluorescence on flat metal surfaces [39–42]. The power-dependent and nonlinear plasmon-enhanced upconversion process has also attracted considerable attention, and effective manipulation and utilization of the upconversion nanocrystals have been the focus of research [43–51]. However, a key issue of plasmon-enhanced cooperative energy transfer in Mn^{2+}-doped (Yb^{3+}, Er^{3+})/$NaYF_4$ has not been addressed. A specific higher-*Q* plasmonic cavity composed of a silver nanorod (AgNR) array can be used to dynamically tune the Mn^{2+}-assisted cooperative emission in order to realize higher tunability of the cooperative energy transfer process in a Mn^{2+}-doped (Yb^{3+}, Er^{3+})/$NaYF_4$ nanocrystal. This also gives a comparison to the Ag nanoparticle film, which has so far not been examined.

In this study, we investigate strong cooperative energy transfer in Mn^{2+}-doped and bare (Yb^{3+}, Er^{3+})/$NaYF_4$ nanocrystals by using a strongly confined plasmonic cavity. The emission ratio I_{655}/I_{540} increases to about 162% and 125%, respectively, for the doped and bare (Yb^{3+}, Er^{3+})/$NaYF_4$ nanocrystals coupled to AgNRs with a resonance wavelength of about 655 nm, as the laser power is increased to 190 mW. The increase indicates an enhancement of the cooperative emissions by plasmon coupling. This also shows that the effect of the doped Mn^{2+} ions on the energy transfer is significantly strengthened by the plasmonic effect. Further, the emission ratio I_{540}/I_{520} increases to about 283% and 267% respectively for the doped and bare (Yb^{3+}, Er^{3+})/$NaYF_4$ nanocrystals coupled to the same AgNRs with a resonance wavelength of about 655 nm, as the laser power is increased to 190 mW. This is attributed to the local field enhancement by the AgNRs. Our new method will have a strong impact in this field and will have prospective applications in the design and preparation of multi-functional rare-earth nanocrystals with highly efficient energy transfers and optical responses. In addition, Mn^{2+} doping into the (Er^{3+}, Yb^{3+}):$NaYF_4$ nanocrystal also has potential use in magnetic sensors [52].

2 Experimental

2.1 Preparation of the sample

Anodic aluminum oxide (AAO) templates were fabricated using a two-step anodization process. First, aluminum sheets (99.999% purity) were degreased in acetone and electropolished under a constant voltage of 16 V for 4 min in a mixture of $HClO_4$ and C_2H_5OH at 0 ℃ to smoothen the sample surface. In the first of two anodization processes, the treated aluminum sheets were immersed in aqueous H_2SO_4 (0.3 mol/L) in an electrochemical cell at about 4 ℃ under a constant voltage of 19 V. The AAO templates were then further anodized by applying potential that was reduced stepwise from 19 to 13 V to decrease the thickness of the alumina barrier layer. Ag nanorods were deposited in the nanopores of the AAO template by alternating current (50 Hz, 7 V AC) electrolysis in an electrolyte composed of $AgNO_3$ (0.03 mol/L) and H_2SO_4 (0.03 mol/L), and a Pt counter electrode was used. The length of the Ag nanorods was controlled by controlling the electrodeposition time. The underlying Al substrate

was then dissolved using a $CuCl_2$ solution.

In a typical procedure, 0.6 g NaOH was dissolved in 3 mL deionized water. With vigorous stirring, 10 mL ethanol and 10 mL oleic acid were added to the NaOH aqueous solution. Then, 4 mL of 0.2 mol/L rare-earth ions Y^{3+}, Yb^{3+}, and Er^{3+} and Mn^{2+} were added into the mixture with a certain percentage. Finally, 2 mL of 2 mol/L NH_4F was added at room temperature while stirring for 15 min. The product was heated in a 50 mL polytetrafluoroethylene reaction kettle for 2 h at 200 ℃. After naturally cooling, the sample was centrifuged with ethanol and water four times, and then dried in a vacuum tank for 12 h at 65 ℃. The sample was then stored for characterization. The resulting Mn^{2+}:(Yb^{3+}, Er^{3+})/$NaYF_4$ was deposited on the AAO template by the spin coating method at a rate of 1,500 rpm for 20 s.

2.2 PL Measurement with plasmonic cavity

The PL from the samples was determined by reflection measurement. A p-polarized laser beam for the measurement of PL was generated by a continuous wave Ti:Sapphire laser (Mira 900, Coherent) and the excitation wavelength was set at ~960 nm. The PL from the sample was collected by a focusing lens and filtered by a couple of filters. The PL spectra were recorded by a spectrometer (Spectrapro 2500i, Acton) using a liquid-nitrogen-cooled CCD.

3 Results and discussion

3.1 Nanostructures and energy transfer of Mn^{2+}:(Yb^{3+}, Er^{3+})/$NaYF_4$

$NaYF_4$ doped with (Yb^{3+}, Er^{3+}) ions has been used to demonstrate the dynamic effect of rare-earth materials, and Mn^{2+} ion doping is an efficient way to tune the morphology and optical properties of (Yb^{3+}, Er^{3+})/$NaYF_4$ nanocrystals. The transmission electron microscope (TEM) images of the (Yb^{3+}, Er^{3+})/$NaYF_4$ undoped and doped with 25% Mn^{2+} ion concentration are shown in Figs. 1(a) and 1(b), respectively. Figure 1(c) shows the energy diagram of Yb^{3+}, Er^{3+}, and Mn^{2+}, which displays the energy transfer channels in our system. There are mainly three channels that correspond to the 520, 540, and 655 nm emission peaks, marked by the pink, blue, and red lines, respectively. They correspond

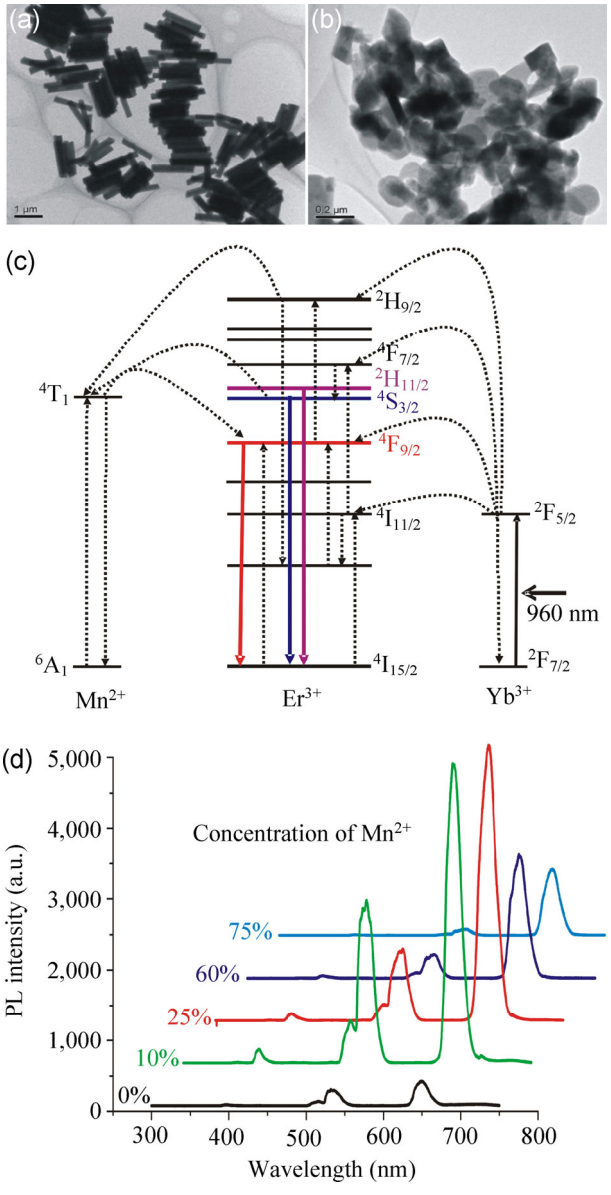

Figure 1 Tunable optical properties of the Mn^{2+}:(Yb^{3+}, Er^{3+})/$NaYF_4$ nanocrystals with different Mn^{2+} concentration. TEM images of (Yb^{3+}, Er^{3+})/$NaYF_4$ nanocrystals with (a) 0% Mn^{2+} and with (b) 25% Mn^{2+}. (c) The energy level diagram of the Yb^{3+}, Er^{3+}, and Mn^{2+} ions. (d) The PL spectra for different concentrations of Mn^{2+}.

to $^2H_{11/2} \rightarrow {}^4I_{15/2}$, $^4S_{3/2} \rightarrow {}^4I_{15/2}$, and $^4F_{9/2} \rightarrow {}^4I_{15/2}$ transitions of Er^{3+}, respectively. The PL spectra and intensity of the (Yb^{3+}, Er^{3+})/$NaYF_4$ nanocrystals also varied with different doping percentages of Mn^{2+}, as shown in Fig. 1(d). The excitation power is 120 mW and the exposure time is 20 ms. The emission ratio I_{655}/I_{540} increases with the amount of Mn^{2+} dopant, which is attributed to the energy transfer channel introduced by the Mn^{2+} ions (energy level $^4T_1$).

3.2 Tuning the upconversion PL of Mn^{2+}:(Yb^{3+}, Er^{3+})/$NaYF_4$ by using AgNR cavity

The plasmon nanocavity prepared using AgNRs was used to investigate the upconversion properties of the Mn^{2+}:(Yb^{3+}, Er^{3+})/$NaYF_4$. The AgNRs were deposited onto an AAO template with the Mn^{2+}:(Yb^{3+}, Er^{3+})/$NaYF_4$ directly spin coated onto it. The structure is shown in Fig. 2(a). The space between the AgNRs is ~50 nm. The average diameter and length of the AgNRs are ~15 and ~50 nm, respectively (shown in Supplementary Material). The distance between the AgNRs and (Yb^{3+}, Er^{3+})/$NaYF_4$ nanocrystals is ~15 nm. Figure 2(b) shows a scanning electron microscope (SEM) image of the nanohole array of the AAO with AgNRs. The local surface plasmon resonance (LSPR) of the AgNRs was tuned to be resonant with the emission peak of the Mn^{2+}:(Yb^{3+}, Er^{3+})/$NaYF_4$ crystal. The above parameters provide the best local field enhancement and energy transfer effect, which has been confirmed by our previous work [53, 54]. The absorption spectra of the AgNR cavity are presented in Fig. 2(c) with the black (θ_{in} = 65°) and red (θ_{in} = 0°) lines, and the blue line is the PL spectrum of the Mn^{2+}:(Yb^{3+}, Er^{3+})/$NaYF_4$ crystal. θ_{in} is the incident angle of the light source for the absorption measurement.

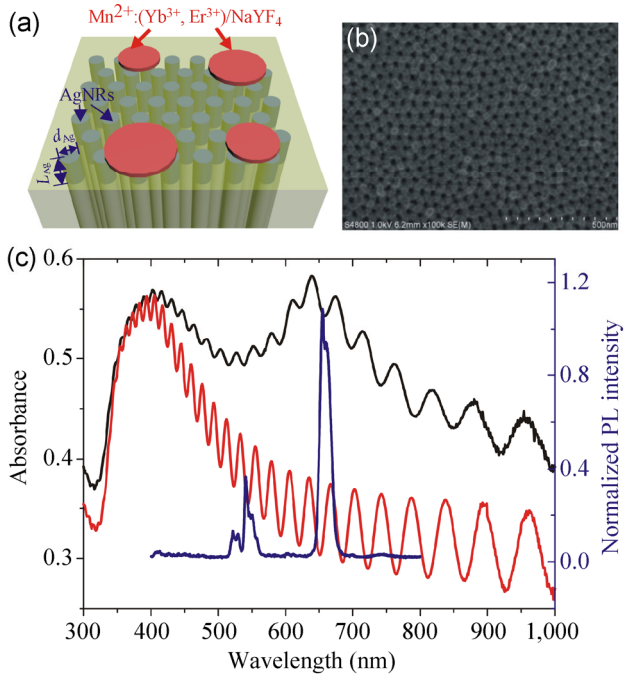

Figure 2 Optical structure of the plasmonic nanocavity. (a) The nanostructure of the sample; the AgNRs were deposited on the AAO template. The Mn^{2+}:(Yb^{3+}, Er^{3+})/$NaYF_4$ nanocrystals were spin coated on the barrier layer side of the AAO template. (b) The SEM image of the nanohole array of the AAO doped with silver nanorods. (c) The absorption spectra of the AgNRs are shown in black (θ_{in} = 65°) and red (θ_{in} = 0°), and the PL spectrum of the Mn^{2+}:(Yb^{3+}, Er^{3+})/$NaYF_4$ crystals appears in blue.

The PL spectra of the (Yb^{3+}, Er^{3+})/$NaYF_4$ doped with 0% Mn^{2+} and 25% Mn^{2+} with PL enhancement by the AgNR cavity are shown in Figs. 3(a) and 3(b), respectively. The excitation power is 30 mW, and the exposed time is 30 ms. An approximately two-fold enhancement was observed in both cases. Plasmonic structures enhance not only the radiative rate but also the non-radiative rate, and the PL enhancement is a cooperative function of these two effects. Owing to the quite large size of the Mn^{2+}:(Yb^{3+}, Er^{3+})/$NaYF_4$ nanocrystal compared to a single Ag nanorod and because of the distance between AgNRs, the PL enhancement in this work is averaged over a large area. Therefore, the positions of the Mn^{2+}:(Yb^{3+}, Er^{3+})/$NaYF_4$ crystals on the AgNR cavity have little influence on the PL enhancement. However, in this study, we mainly focus on the enhancement in the energy transfer process between Mn^{2+} and Er^{3+} due to the plasmon cavity, which has an insignificant relation to the non-radiative decay in the metallic parts.

The PL spectra of the Mn^{2+}:(Yb^{3+}, Er^{3+})/$NaYF_4$ with AgNR cavity as a function of excitation power are shown in Fig. 4(a). We can observe that the PL intensities of the three peaks around 520, 540, and 655 nm increase with excitation power but at different rates. The PL intensities of the three peaks as a function of the excitation power are presented in Fig. 4(b). The corresponding slopes, $\nu = \partial \log I_{emi}/\partial \log I_{exc}$, of the 520, 540, and 655 nm peaks are 1.70, 1.35, and 1.61, respectively. The ratios of I_{655}/I_{540} and I_{520}/I_{540} increase with the excitation power, as shown in Figs. 4(c) and 4(d). I_{655}/I_{540} for the (Yb^{3+}, Er^{3+})/$NaYF_4$ sample with the AgNR cavity increases much more rapidly with the excitation power than that for the (Yb^{3+}, Er^{3+})/$NaYF_4$ sample without the AgNR cavity does; this confirms that these ratio changes can be attributed to field enhancement and energy transfer induced by the AgNR cavity (shown in Fig. 4(c)). This is because multiple energy transfer channels have been introduced

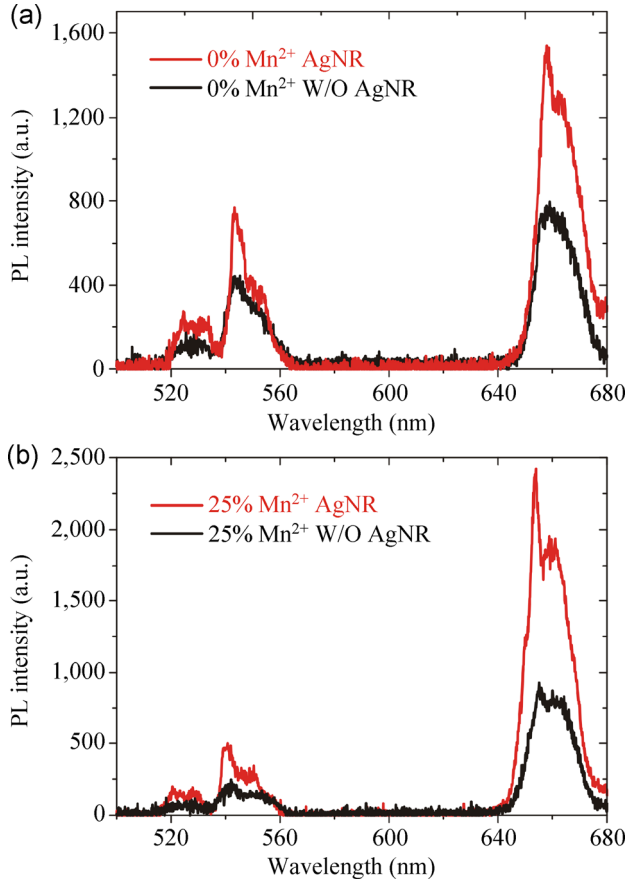

Figure 3 The PL enhancement of the (Yb^{3+}, Er^{3+})/$NaYF_4$ crystals doped with (a) 0% Mn^{2+} and (b) 25% Mn^{2+} with (red line) and without (black line) AgNRs. The LSPR of AgNRs is ~655 nm.

due to doping of Mn^{2+} ions (energy level $^4T_1$). The excited electrons in the $^4S_{3/2}$ state would transfer to the $^4T_1$ energy level and then to $^4F_{9/2}$, which will increase the red emission of the sample and thus increase the emission ratio I_{655}/I_{540}. The local electric field induced by the plasmonic AgNR nanocavity enhances the energy transfer process and this leads to larger values of the ratio. On the other hand, Mn^{2+} doping can only slightly increase I_{520}/I_{540} (Fig. 4(d)) when the AgNRs are absent. I_{520}/I_{540} remains almost unchanged with the increase in the excitation power. However, when AgNRs are introduced into the samples, the ratios increase rapidly. This is ascribed to the large field enhancement by the plasmon resonance in the nanocavity.

Plasmons enhance the energy transfer rate between Mn^{2+} and (Yb^{3+}, Er^{3+}) as well as the final radiative efficiency of Er^{3+}, since the Mn^{2+}-doped (Yb^{3+}, Er^{3+})/$NaYF_4$ has much larger I_{655}/I_{540} and I_{520}/I_{540} ratios. More

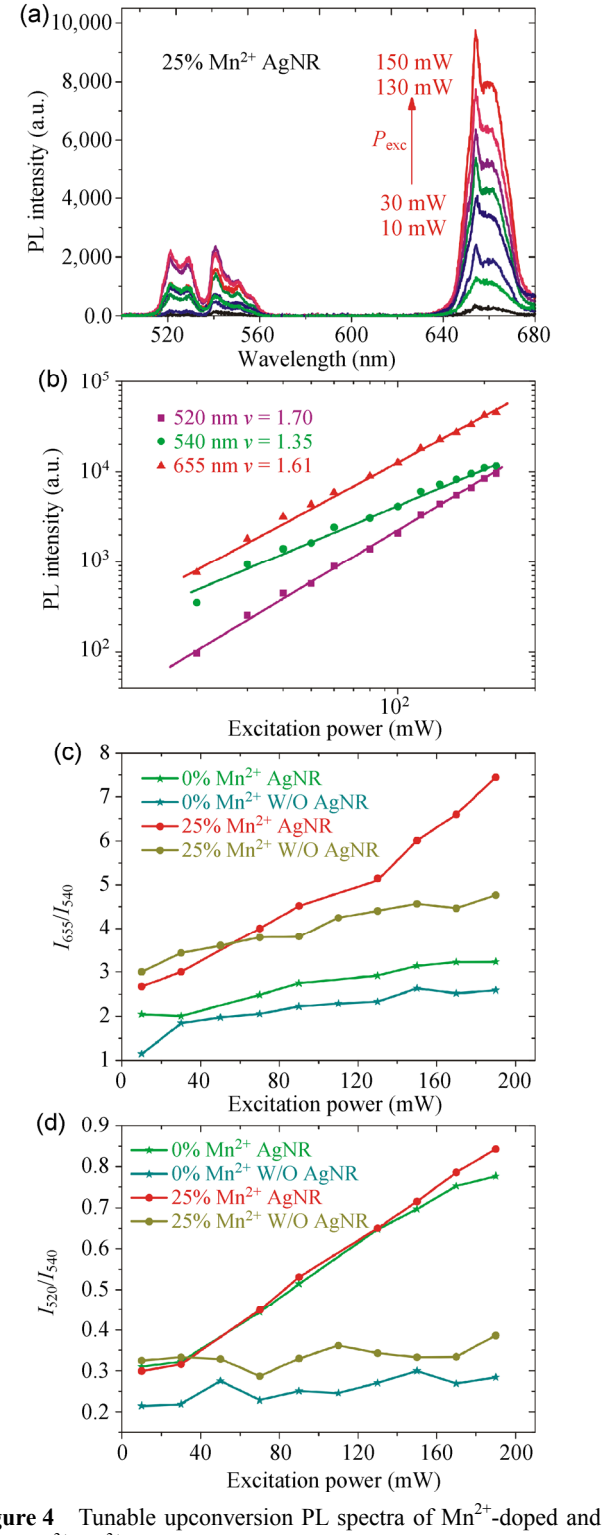

Figure 4 Tunable upconversion PL spectra of Mn^{2+}-doped and bare (Yb^{3+}, Er^{3+})/$NaYF_4$ nanocrystals coupled to plasmonic nanocavity. (a) The PL spectra dependence on the excitation power of the (Yb^{3+}, Er^{3+})/$NaYF_4$ on the AgNR cavity. (b) The PL intensity dependence of the three peaks (520, 540, and 655 nm) on the excitation power. The PL intensity ratios (c) I_{655}/I_{540} and (d) I_{540}/I_{520} as a function of the excitation power; the brown and dark green lines show the results without the AgNRs.

specifically, the emission ratio I_{520}/I_{540} is increased by the enhanced energy transfer from Mn^{2+} to Er^{3+}, while the emission ratio I_{655}/I_{540} is increased by the collaborative enhancements of the energy transfer and emission efficiency. The sample with the AgNR cavity has a much larger power-dependent increase in I_{655}/I_{540} than a Ag nanoparticle film (shown in Supplementary Material), which highlights the significant nonlinear gain of the plasmon cavity coupled to the activated optical dipoles. This nonlinear energy transfer can be further improved by optimizing the design of the plasmonic nanocavity and improving the coupling between the cavity and fluorescent ions.

4 Conclusions

This work provides a systematic investigation of the tunability of cooperative energy transfer and nonlinear upconversion emissions of (Yb^{3+}, Er^{3+})/$NaYF_4$ nanocrystals (undoped and doped with Mn^{2+} ions) both with and without a AgNR plasmonic nanocavity. The emission ratios I_{655}/I_{540} and I_{520}/I_{540} for the doped and bare (Yb^{3+}, Er^{3+})/$NaYF_4$ nanocrystals coupled to the plasmonic cavity increase with the excitation laser power. This indicates a very efficient enhancement of the cooperative emissions by the plasmon field. This further demonstrates that the energy transfer is largely enhanced by the plasmonic cavity. Our observations have prospective applications in designing and preparing multi-functional rare-earth nanocrystals with highly efficient energy transfer and excellent optical responses.

Acknowledgements

We thank Haiyang Li for her assistance in sample preparation, Li Zhou for assistance in the laboratory. This work was supported in part by the National Natural Science Foundation of China (Nos. 11404124, 11174229, and 11204221), the National Basic Research Program of China (No. 2011CB922200), the Ministry of Science and Technology of China (No. 2012YQ12006005), the U.S. DOE (Division of Materials Sciences and Engineering, Office of Basic Energy Sciences), and by the U.S. NSF (No. DMR-0906025).

Electronic Supplementary Material: Supplementary material (the data of Ag nanoparticle films) is available in the online version of this article at http://dx.doi.org/10.1007/s12274-015-0802-2.

References

[1] Mao, Y. B.; Huang, J. Y.; Ostroumov, R.; Wang, K. L.; Chang, J. P. Synthesis and luminescence properties of erbium-doped Y_2O_3 nanotubes. *J. Phys. Chem. C* **2008**, *112*, 2278–2285.

[2] Mao, Y. B.; Tran, T.; Guo, X.; Huang, J. Y.; Shih, C. K.; Wang, K. L.; Chang, J. P. Luminescence of nanocrystalline erbium-doped yttria. *Adv. Func. Mater.* **2009**, *19*, 748–754.

[3] Ye, X. C.; Collins, J. E.; Kang, Y. J.; Chen, J.; Chen, D. T. N.; Yodh, A. G.; Murray, C. B. Morphologically controlled synthesis of colloidal upconversion nanophosphors and their shape-directed self-assembly. *Proc. Natl. Acad. Sci. USA* **2010**, *107*, 22430–22435.

[4] Gai, S. L.; Li, C. X.; Yang, P. P.; Lin, J. Recent progress in rare earth micro/nanocrystals: Soft chemical synthesis, luminescent properties, and biomedical applications. *Chem. Rev.* **2014**, *114*, 2343–2389.

[5] Chen, G. Y.; Qiu, H. L.; Prasad, P. N.; Chen, X. Y. Upconversion nanoparticles: Design, nanochemistry, and applications in theranostics. *Chem. Rev.* **2014**, *114*, 5161–5214.

[6] Huang, X. Y.; Han, S. Y.; Huang, W.; Liu, X. G.Enhancing solar cell efficiency: The search for luminescent materials as spectral converters. *Chem. Soc. Rev.* **2013**, *42*, 173–201.

[7] Zhang, F.; Wan, Y.; Yu, T.; Zhang, F. Q.; Shi, Y. F.; Xie, S. H.; Li, Y. G.; Xu, L.; Tu, B.; Zhao, D. Y. Uniform nanostructured arrays of sodium rare-earth fluorides for highly efficient multicolor upconversion luminescence. *Angew. Chem., Int. Ed.* **2007**, *46*, 7976–7979.

[8] Yu, X. F.; Chen, L. D.; Li, M.; Xie, M. Y.; Zhou, L.; Li, Y.; Wang, Q. Q. Highly efficient fluorescence of NdF_3/SiO_2 core/shell nanoparticles and the applications for *in vivo* NIR detection. *Adv. Mater.* **2008**, *20*, 4118–4123.

[9] Ehlert, O.; Thomann, R.; Darbandi, M.; Nann, T. A four-color colloidal multiplexing nanoparticle system. *ACS Nano* **2008**, *2*, 120–124.

[10] Yi, G. S.; Lu, H. C.; Zhao, S. Y.;Ge, Y.; Yang, W. J.;Chen, D. P.; Guo, L. H. Synthesis, characterization, and biological application of size-controlled nanocrystalline $NaYF_4$:Yb,Er infrared-to-visible upconversion phosphors. *Nano Lett.* **2004**, *4*, 2191–2196.

[11] Chatterjee, D. K.; Rufaihah, A. J.; Zhang, Y. Upconversion fluorescence imaging of cells and small animals using lanthanide doped nanocrystals. *Biomaterials* **2008**, *29*, 937–943.

[12] Nyk, M.; Kumar, R.; Ohulchanskyy, T. Y.; Bergey, E. J.; Prasad, P. N. High contrast *in vitro* and *in vivo* photoluminescence bioimaging using near infrared to near infrared upconversion in Tm^{3+} and Yb^{3+} doped fluoride nanophosphors. *Nano Lett.* **2008**, *8*, 3834–3838.

[13] Heer, S.; Kömpe, K.; Güdel, H. U.; Haase, M. Highly efficient multicolor upconversion emission in transparent colloids of lanthanide-doped $NaYF_4$ nanocrystals. *Adv. Mater.* **2004**, *16*, 2102–2105.

[14] Wang, F.; Liu, X. G.Upconversion multicolor fine-tuning: Visible to near infrared emission from lanthanide-doped $NaYF_4$ nanoparticles. *J. Am. Chem. Soc.* **2008**, *130*, 5642–5643.

[15] Shalav, A.; Richards, B. S.; Trupke, T.; Krämer, K. W.; Güdel, H. U. Application of $NaYF_4$:Er^{3+} up-converting phosphors for enhanced near-infrared silicon solar cell response. *Appl. Phys. Lett.* **2005**, *86*, 013505.

[16] van der Ende, B. M.; Aarts, L.; Meijerink, A. Lanthanide ions as spectral converters for solar cells. *Phys. Chem. Chem. Phys.* **2009**, *11*, 11081–11095.

[17] Wang, H. Q.; Batentschuk, M.; Osvet, A.; Pinna, L.; Brabec, C. J. Rare-earth ion doped up-conversion materials for photovoltaic applications. *Adv. Mater.* **2011**, *23*, 2675–2680.

[18] Gorris, H. H.; Ali, R.; Saleh, S. M.; Wolfbeis, O. S. Tuning the dual emission of photon-upconverting nanoparticles for ratiometric multiplexed encoding. *Adv. Mater.* **2011**, *23*, 1652–1655.

[19] Miyakawa, T.; Dexter, D. L. Cooperative and stepwise excitation of luminescence: Trivalent rare-earth ions in Yb^{3+}-sensitized crystals. *Phys. Rev. B* **1970**, *1*, 70–80.

[20] Tian, G.; Gu, Z. J.; Zhou, L. J.; Yin, W. Y.; Liu, X. X.; Yan, L.; Jin, S.; Ren, W. L.; Xing, G. M.; Li, S. J. et al. Mn^{2+} dopant-controlled synthesis of $NaYF_4$:Yb/Er upconversion nanoparticles for *in vivo* imaging and drug delivery. *Adv. Mater.* **2012**, *24*, 1226–1231.

[21] Bai, Z. H.; Lin, H.; Johnson, J.; Gui, S. C. R.; Imakita, K.; Montazami, R.; Fujii, M.; Hashemi, N. The single-band red upconversion luminescence from morphology and size controllable Er^{3+}/Yb^{3+} doped MnF_2 nanostructures. *J. Mater. Chem. C* **2014**, *2*, 1736–1741.

[22] Wang, J.; Wang, F.; Wang, C.; Liu, Z.; Liu, X. G.Single-band upconversion emission in lanthanide-doped $KMnF_3$ nanocrystals. *Angew. Chem., Int. Ed.* **2011**, *50*, 10369–10372.

[23] Chen, G. Y.; Liu, Y.; Zhang, Y. G.; Somesfalean, G.; Zhang, Z. G.; Sun, Q.; Wang, F. P. Bright white upconversion luminescence in rare-earth-ion-doped Y_2O_3 nanocrystals. *Appl. Phys. Lett.* **2007**, *91*, 133103.

[24] Wang, F.; Deng, R. R.; Wang, J.; Wang, Q. X.; Han, Y.; Zhu, H. M.; Chen, X. Y.; Liu, X. G.Tuning upconversion through energy migration in core–shell nanoparticles. *Nat. Mater.* **2011**, *10*, 968–973.

[25] Su, Q. Q.; Han, S. Y.; Xie, X. J.; Zhu, H. M.; Chen, H. Y.; Chen, C.-K.; Liu, R.-S.; Chen, X. Y.; Wang, F.; Liu, X. G. The effect of surface coating on energy migration-mediated upconversion. *J. Am. Chem. Soc.* **2012**, *134*, 20849–20857.

[26] Chen, G. Y.; Ohulchanskyy, T. Y.; Kachynski, A.; Ågren, H.; Prasad, P. N. Intense visible and near-infrared upconversion photoluminescence in colloidal $LiYF_4$:Er^{3+} nanocrystals under excitation at 1490 nm. *ACS Nano* **2011**, *5*, 4981–4986.

[27] Song, E. H.; Ding, S.; Wu, M.; Ye, S.; Xiao, F.; Dong, G. P.; Zhang, Q. Y. Temperature-tunable upconversion luminescence of pervskite nanocrystals $KZnF_3$:Yb^{3+},Mn^{2+}. *J. Mater. Chem. C* **2013**, *1*, 4209–4215.

[28] Jackson, J. B.; Halas, N. J. Surface-enhanced Raman scattering on tunable plasmonic nanoparticle substrates. *Proc. Natl. Acad. Sci. USA* **2004**, *101*, 17930–17935.

[29] Nan, F.; Cheng, Z. Q.; Wang, Y. L.; Zhang, Q.; Zhou, L.; Yang, Z. J.; Zhong, Y. T.; Liang, S.; Xiong, Q. H.; Wang, Q. Q. Manipulating nonlinear emission and cooperative effect of CdSe/ZnS quantum dots by coupling to a silver nanorod complex cavity. *Sci. Rep.* **2014**, *4*, 4839.

[30] Hillenbrand, R.; Taubner, T.; Keilmann, F. Phonon-enhanced light–matter interaction at the nanometre scale. *Nature* **2002**, *418*, 159–162.

[31] Schuller, J. A.; Barnard, E. S.; Cai, W. S.; Jun, Y. C.; White, J. S.; Brongersma, M. L. Plasmonics for extreme light concentration and manipulation. *Nat. Mater.* **2010**, *9*, 193–204.

[32] Maier, S. A.; Kik, P. G.; Atwater, H. A.; Meltzer, S.; Harel, E.; Koel, B. E.; Requicha, A. A. G. Local detection of electromagnetic energy transport below the diffraction limit in metal nanoparticle plasmon waveguides. *Nat. Mater.* **2003**, *2*, 229–232.

[33] Saboktakin, M.; Ye, X. C.; Oh, S. J.; Hong, S. H.; Fafarman, A. T.; Chettiar, U. K.; Engheta, N.; Murray, C. B.; Kagan, C. R. Metal-enhanced upconversion luminescence tunable through metal nanoparticle–nanophosphor separation. *ACS Nano* **2012**, *6*, 8758–8766.

[34] Saboktakin, M.; Ye, X. C.; Chettiar, U. K.; Engheta, N.; Murray, C. B.; Kagan, C. R. Plasmonic enhancement of nanophosphor upconversion luminescence in Au nanohole arrays. *ACS Nano* **2013**, *7*, 7186–7192.

[35] Greybush, N. J.; Saboktakin, M.; Ye, X. C.; Della Giovampaola, C.; Oh, S. J.; Berry, N. E.; Engheta, N.; Murray, C. B.; Kagan, C. R. Plasmon-enhanced upconversion luminescence in single nanophosphor–nanorod heterodimers formed through template-assisted self-assembly. *ACS Nano* **2014**, *8*, 9482–9491.

[36] Yuan, P. Y.; Lee, Y. H.; Gnanasammandhan, M. K.; Guan, Z. P.; Zhang, Y.; Xu, Q. H. Plasmon enhanced upconversion

luminescence of $NaYF_4$:Yb,Er@SiO_2@Ag core-shell nanocomposites for cell imaging. *Nanoscale* **2012**, *4*, 5132–5137.

[37] Schietinger, S.; Aichele, T.; Wang, H. Q.; Nann, T.; Benson, O. Plasmon-enhanced upconversion in single $NaYF_4$:Yb^{3+}/Er^{3+} codoped nanocrystals. *Nano Lett.* **2009**, *10*, 134–138.

[38] Schietinger, S.; Menezes, L. de S.; Lauritzen, B.; Benson, O. Observation of size dependence in multicolor upconversion in single Yb^{3+}, Er^{3+} codoped $NaYF_4$ nanocrystals. *Nano Lett.*, **2009**, *9*, 2477–2481.

[39] Zhang, H.; Li, Y. J.; Ivanov, I. A.; Qu, Y. Q.; Huang, Y.; Duan, X. F. Plasmonic modulation of the upconversion fluorescence in $NaYF_4$:Yb/Tm hexaplate nanocrystals using gold nanoparticles or nanoshells. *Angew. Chem.* **2010**, *122*, 2927–2930.

[40] Li, Z. Q.; Wang, L. M.; Wang, Z. Y.; Liu, X. H.; Xiong, Y. J. Modification of $NaYF_4$:Yb,Er@SiO_2 nanoparticles with gold nanocrystals for tunable green-to-red upconversion emissions. *J. Phys. Chem. C* **2011**, *115*, 3291–3296.

[41] Wawrzynczyk, D.; Bednarkiewicz, A.; Nyk, M.; Gordel, M.; Strek, W.; Samoc, M.Modulation of up-conversion luminescence of lanthanide(III) ion co-doped $NaYF_4$ nanoparticles using gold nanorods. *Opt. Mater.* **2012**, *34*, 1708–1712.

[42] Wang, F.; Liu, X. G.Upconversion multicolor fine-tuning: Visible to near-infrared emission from lanthanide-doped $NaYF_4$ nanoparticles. *J. Am. Chem. Soc.* **2008**, *130*, 5642–5643.

[43] Sun, Q. C.; Mundoor, H.; Ribot, J. C.; Singh, V.; Smalyukh, I. I.; Nagpal, P. Plasmon-enhanced energy transfer for improved upconversion of infrared radiation in doped-lanthanide nanocrystals. *Nano Lett.* **2014**, *14*, 101–106.

[44] Pollnau, M.; Gamelin, D. R.; Lüthi, S. R.; Güdel, H. U.; Hehlen, M. P. Power dependence of upconversion luminescence in lanthanide and transition-metal-ion systems. *Phys. Rev. B* **2000**, *61*, 3337–3346.

[45] Zhang, H.; Xu, D.; Huang, Y.; Duan, X. F.Highly spectral dependent enhancement of upconversion emission with sputtered gold island films. *Chem. Commun.* **2011**, *47*, 979–981.

[46] Verhagen, E.; Kuipers, L.; Polman, A. Enhanced nonlinear optical effects with a tapered plasmonic waveguide. *Nano Lett.* **2007**, *7*, 334–337.

[47] Paudel, H. P.; Zhong, L. L.; Bayat, K.; Baroughi, M. F.; Smith, S.; Lin, C. K.; Jiang, C. Y.; Berry, M. T.; May, P. S. Enhancement of near-infrared-to-visible upconversion luminescence using engineered plasmonic gold surfaces. *J. Phys. Chem. C* **2011**, *115*, 19028–19036.

[48] Wang, G. F.; Qin, W. P.; Wang, L. L.; Wei, G. D.; Zhu, P. F.; Kim, R. Intense ultraviolet upconversion luminescence from hexagonal $NaYF_4$: Yb^{3+}/Tm^{3+} microcrystals. *Opt. Express* **2008**, *16*, 11907–11914.

[49] Suyver, J. F.; Grimm, J.; van Veen, M. K.; Biner, D.; Krämer, K. W.; Güdel, H. U. Upconversion spectroscopy and properties of $NaYF_4$ doped with Er^{3+}, Tm^{3+} and/or Yb^{3+}. *J. Lumin.* **2006**, *117*, 1–12.

[50] Shan, J. N.; Uddi, M.; Wei, R.; Yao, N.; Ju, Y. G.The hidden effects of particle shape and criteria for evaluating the upconversion luminescence of the lanthanide doped nanophosphors. *J. Phys. Chem. C* **2010**, *114*, 2452–2461.

[51] Krämer, K. W.; Biner, D.; Frei, G.; Güdel, H. U.; Hehlen, M. P.; Lüthi, S. R. Hexagonal sodium yttrium fluoride based green and blue emitting upconversion phosphors. *Chem. Mater.* **2004**, *16*, 1244–1251.

[52] Wang,Y. L.; Zhang,J. P.; Han,J. B.; Hao,Z. H.; WangQ. Q. High magnetic field and temperature tuning of up-conversion luminescence in Mn^{2+}-doped (Er^{3+}/Yb^{3+}): $NaYF_4$. *J. Appl. Phys.* **2015**, *117*, 083903.

[53] Zhou, Z. K.; Peng, X. N.; Yang, Z. J.; Zhang, Z. S.; Li, M.; Su, X. R.; Zhang, Q.; Shan, X. Y.; Wang, Q. Q.; Zhang, Z. Y. Tuning gold nanorod-nanoparticle hybrids into plasmonic Fano resonance for dramatically enhanced light emission and transmission. *Nano Lett.* **2011**, *11*, 49–55.

[54] Zhou, Z. K.; Li, M.; Yang, Z. J.; Peng, X. N.; Su, X. R.; Zhang, Z. S.; Li, J. B.; Kim, N. C.; Yu, X. F.; Zhou, L. et al. Plasmon-mediated radiative energy transfer across a silver nanowire array via resonant transmission and subwavelength imaging. *ACS Nano* **2010**, *4*, 5003–5010.